Disturbance observer-based adaptive neural guidance and control of an aircraft using composite learning

Disturbance observer-based adaptive neural guidance and control of an aircraft using composite learning

Seyyed Ali Emami [a], Afshin Banazadeh [a,*], Pedram Hajipourzadeh [a], Paolo Castaldi [b], S. Ahmad Fazelzadeh [c]

[a] Department of Aerospace Engineering, Sharif University of Technology, Tehran, Iran
[b] Department of Electrical, Electronic and Information Engineering "Guglielmo Marconi", University of Bologna, Via Dell'Università 50, Cesena, Italy
[c] Department of Mechanical Engineering, Shiraz University, Shiraz, Iran

ARTICLE INFO

Keywords:
Aerial robot control
Composite real-time learning
Guidance loop
Intelligent flight control
Neural Networks

ABSTRACT

An adaptive neural guidance and control system is proposed in this paper for a generic fixed-wing aerial robot. Unlike most of the existing low-level control systems, which utilize a non-adaptive guidance loop, in this work both the guidance and control loops are trained using an efficient adaptive neural algorithm. A feedforward neural network is employed in each loop to identify uncertain dynamics, while an adaptive disturbance observer allows to compensate for both the external disturbances and estimation error of the neural network. This would lead to a resilient flight control system, and thus, the asymptotic stability of both the guidance and control loops can be theoretically ensured for a generic aerial robot subject to different types of nonparametric internal and external disturbances. Besides, to enhance the learning efficiency, a composite learning method is adopted in which the neural network and the disturbance observer are trained using a composite error function consisting of the tracking error and the estimation error of an introduced adaptive state observer. To the best of the authors' knowledge, this is the first completely adaptive integrated guidance and control system with guaranteed stability under parametric and nonparametric internal and external disturbances. The introduced control system is then applied to a simulation model of an electric aircraft that has been validated on the basis of real data and flight experiments. The obtained results indicate that the proposed approach could be considered a reliable guidance and control system for a generic fixed-wing aerial vehicle in the presence of actuator faults, unmodeled dynamics, external disturbances, and measurement noises.

1. Introduction

Neural Networks (NNs) have been extensively utilized in adaptive control systems in the last two decades, particularly, in the case of aerial robotic vehicles (Kacprzyk, Schumann, & Liu, 2010; Pi, Hu, Cheng, & Wu, 2020). Due to their unique features, such as the universal approximation property and effective learning capability, they can satisfactorily deal with both *parametric* and *nonparametric* model uncertainties (Emami & Banazadeh, 2019; Emami & Roudbari, 2019). Another important feature of NNs compared to basic fuzzy systems is the lack of necessity for prior information about the system dynamics in the learning process (Lee, 1990; Zahmatkesh, Emami, Banazadeh, & Castaldi, 2022), thereby providing significant potential to be employed in the case of complex control problems.

NNs can be integrated with different learning methodologies, and due to their inherent parallel processing property, they can be effectively used in real-time implementations (Campa et al., 2002; Kacprzyk et al., 2010). Feedback Error Learning (FEL) is known as the most common approach to involve NNs in the structure of an adaptive control design (Gomi & Kawato, 1993; Wang et al., 2018). Such control methods are also known as a variety of intelligent control systems, owing to the ability of the controller to learn and compensate for unknown dynamics in the system and environment (Emami, Castaldi, & Banazadeh, 2022). FEL can be employed to compensate for the effect of model uncertainties by taking advantage of the *tracking error* in the updating rule of the NN while satisfying the Lyapunov stability criteria. Further, it can be satisfactorily employed in both direct and indirect intelligent controllers.

1.1. Existing neural control methodologies

To be more specific, if the dynamic model of a system can be represented as $\dot{x} = F(x) + B(x)u + \Delta(x)$ with Δ denoting an unknown function of system states, it is possible to estimate it (in an appropriate compact set) using a NN as $\hat{\Delta} = \hat{W}^T \mu(x)$, where $\mu(x)$ and $\hat{W}$ represent,

* Corresponding author.
E-mail address: banazadeh@sharif.edu (A. Banazadeh).

respectively, an appropriate basis function vector (or matrix) and the output weights, which should be trained by FEL. Accordingly, in such a control design, it is assumed that a nominal model of the system, i.e. $F(x)$ and $B(x)$ is available. Besides, in the presence of actuator faults, the uncertain term becomes a function of both the system states x and system inputs u. Thus, it is necessary to estimate it as $\hat{\Delta}(x,u) = \hat{W}^T\mu(x,u)$, and as a consequence, the control command becomes a function itself, i.e. $u = h(.,u)$. Such a formulation necessitates a contraction assumption, which implicitly requires the sign of the control gain function to be known (Chowdhary, Mühlegg, & Johnson, 2014). However, such an adaptive control framework suffers from the well-known limitations of aggressive learning (caused by increasing the learning rate), which is a typical approach to compensate for the model inversion error (Gu, Valavanis, Rutherford, & Rizzo, 2019). Another concern with the basic FEL neural control is that the convergence of the NN weights to their optimal values requires persistent excitation (Kacprzyk et al., 2010). Otherwise, the network's parameters are exposed to the well-known parameter drift issue, which in turn, results in a high-gain control scheme (Ge & Wang, 2002). Although different modifications such as the sigma-modification (Ioannou & Sun, 2012), e-modification (Narendra & Annaswamy, 1987), or the projection algorithm (MacKunis, Leve, Patre, Fitz-Coy, & Dixon, 2016) have been introduced in the literature to prevent parameter drift, the principal problem, i.e. the inefficient learning process in the absence of persistent excitation, is not solved using such modifications.

1.2. Composite learning scheme

As an attractive idea to enhance the efficiency of the learning process, it is possible to develop a state observer by taking advantage of the estimated uncertainties, and subsequently, involve the estimation error of the state observer in the learning rule. Such an approach, which is typically known as a *composite learning* scheme (Xu, Shi, Yang, & Sun, 2014; Yu, Zhang, Jiang, Su et al., 2020), has been employed in several flight control systems, particularly, in the case of hypersonic flight vehicles (Xu, Shi, Sun, & He, 2019; Xu, Wang, Zhang, & Shi, 2017). However, only the longitudinal dynamics of the aerial vehicle have been considered in these papers. Moreover, the utilization of an adaptive Disturbance Observer (DO) to compensate for both the estimation error of the NN and the time-dependent disturbances, which cannot be captured by the NN, can effectively eliminate the need for a high learning rate and result in the asymptotic stability of the system as well (Fu et al., 2018; Lai, Liu, Zhang, & Chen, 2016).

1.3. Disturbance observers

High-Gain Observers have been widely used in the literature to estimate unknown system states (He, Yan, Sun, & Chen, 2017; Seshagiri & Khalil, 2000; Xu, Gao, & Wang, 2011). However, they suffer from various issues corresponding to high-gain learning and control (Ioannou et al., 2014). Also, they suffer from the peaking phenomenon (Khalil, 2008), which can even destabilize the system. Similar high-gain filters have been employed in Chakrabortty and Arcak (2009) to deal with unmodeled input dynamics in the control of nonlinear systems, while the designed controller results in significant chattering, which is a problematic issue in practical applications and can saturate the control inputs.

Another type of disturbance observer has been employed in Chen, Shi, and Lim (2016), Yu, Zhang, Jiang, Yu et al. (2020) and Yu, Zhang, Jiang, Su et al. (2020) in combination with NNs in which the DO attempts to estimate the residual uncertain term (which has not been identified by the NN), itself, not the upper bound of that. However, such a design requires an additional assumption on the boundedness of the time-derivative of the disturbance term.

1.4. Adaptive guidance systems

On the other hand, as discussed in Chowdhary, Johnson, Chandramohan, Kimbrell, and Calise (2013), in most existing flight control systems, the guidance loop, which should provide the reference attitude or velocity to be followed by the inner control loop, does not typically consider uncertain terms (including sensor faults, measurement noises, and model uncertainties) in the design. This can lead to a conservative design in the presence of significant changes in the system dynamics model. Thus, there is a need for an adaptive guidance loop, which is capable of modifying the commanded attitude (or velocity) based on the current system conditions. Although a state-dependent guidance law has been proposed in Chowdhary et al. (2013) to ensure that a feasible trajectory is commanded to the aerial vehicle in the presence of structural damages, no theoretical stability analysis has been presented in the paper for the introduced closed-loop system. Besides, an adaptive neural backstepping control has been introduced in Yu, Zhang, Jiang, Su et al. (2020) to provide a decentralized control system for a group of unmanned aerial vehicles in the presence of actuator faults and external disturbances. However, the trajectory tracking control problem (in a 3D environment) has not been addressed in the paper, and the control objective was to follow a reference bank angle, angle of attack, and sideslip angle.

Motivated by the above discussion, an adaptive fault-tolerant guidance and control scheme is developed in this paper using a novel combined FEL neural control and a disturbance observer in both the inner and outer control loops.

1.5. Main contributions of the proposed method

The main contributions of the paper can be summarized as follows:

1. A combination of FEL-based neural control and disturbance observers is developed for a generic fixed-wing aerial robot with nonparametric uncertainties, unmodeled dynamics, actuator faults, and external disturbances. As will be shown, such a combination along with employing a composite learning scheme can effectively tackle considerable actuator faults and external disturbances.
2. A novel, simple, and adaptive guidance algorithm is introduced for a generic fixed-wing air vehicle without the requirement to directly control the angle of attack and the sideslip angle. The guidance loop is integrated with an inner control loop to provide a trajectory tracking control scheme, where the stability of each loop can be separately analyzed using the time-scale decomposition assumption.
3. The closed-loop stability is carefully analyzed using the Lyapunov stability theorem for both the guidance and control loops. Using the proposed DO, the closed-loop system is capable of compensating for both the NN's estimation error and time-dependent external disturbances. Accordingly, the *asymptotic stability* of the closed-loop system would be ensured. In addition, thanks to the employment of the NNs to compensate for uncertain dynamics, the chattering phenomenon due to the signum function, which is a crucial challenge in the use of discontinuous control systems such as the sliding mode control, is significantly reduced (Xian, Diao, Zhao, & Zhang, 2015). Moreover, different from Arabi et al. (2019), which attempted to keep the system trajectory in a compact set that the universal approximation property of the NN is valid, here, the introduced adaptive DO can effectively bring the system trajectory into the mentioned compact set from outside assuming that the uncertain term $\Delta(x,u)$ is bounded.
4. Using the introduced composite learning algorithm, both the *tracking* and *estimation* errors are asymptotically converged to

zero even considering significant internal and external disturbances, while there is no need for an indirect Recursive Least-Squares optimization scheme (as a fault detection and isolation block) (Abbaspour, Aboutalebi, Yen, & Sargolzaei, 2017; Ali Emami & Banazadeh, 2020; Nguyen, Krishnakumar, Kaneshige, & Nespeca, 2008) which can make the stability analysis of the closed-loop system a serious challenge.

5. To evaluate the performance of the proposed control scheme, a detailed nonlinear simulation of a 25 percent dynamically similar model of a newly designed electric aircraft that benefits from distributed propulsion system would be employed, while the model has been validated based on real data and flight experiments.

The remainder of the paper is organized as follows: The problem description is presented in Section 2 in detail, whereas the control design procedure is given in Section 3. Section 4 includes the simulation results, and finally, Section 5 concludes the paper.

2. Problem formulation

The 6-Degrees of Freedom (DOF) nonlinear dynamic model of an aerial robot can be generally formulated as (Emami & Rezaeizadeh, 2018; Galffy, Böck, & Kugi, 2019):

$$\dot{\omega} = I^{-1}\left(M_b - \omega \times I\omega\right), \tag{1}$$

$$\dot{v}_b = \frac{F_b}{m} - \omega \times v_b, \tag{2}$$

where $v_b = [U, V, W]^T$, m, and I represent the aircraft velocity in the body coordinate system, the total vehicle mass, and the moment of inertia matrix, respectively. Also, $\times$ stands for the cross-product operation. In addition, F_b and M_b denote, respectively, the total forces and moments acting on the vehicle (represented in the body coordinate system), which in turn are functions of the control surface deflections, i.e., $u = [\delta_e, \delta_a, \delta_r]^T$ and the throttle setting (δ_T). Here, δ_e, δ_a, and δ_r represent the elevator, the aileron, and the rudder deflection, respectively.

In the case of a trajectory tracking problem, the control objective is to design a control system such that the tracking error $e_r(t) = r(t) - r_d(t)$ converges to zero (or a compact neighborhood of zero), where $r(t) = [x_I, y_I, z_I]^T$ and $r_d(t) = [x_{Id}, y_{Id}, z_{Id}]^T$ denote the vehicle's trajectory and the reference trajectory in the inertial reference frame, respectively.

In this regard, in the following, we will design a multi-loop control system in which the reference trajectory is first transformed into the desired attitude in the outer control loop (guidance loop), and subsequently, the inner loop attempts to control the vehicle's attitude.

More precisely, the problem would be addressed in two consecutive steps. In the first step, an adaptive guidance algorithm is introduced to determine the desired Euler angles' rate and the desired velocity based on the trajectory tracking error. Afterward, in the second step (i.e., the inner control loops, which correspond to the attitude and velocity control systems), appropriate control surface deflections (u) would be determined such that the air vehicle can follow the desired attitude (computed in the first step), and a distinct velocity controller is also proposed to adjust the vehicle's velocity. Using such a framework, the aircraft velocity is adjusted using the throttle setting, and the vehicle's attitude is controlled by control surface deflections, while the coupled dynamics of the attitude and velocity subsystems are dealt with as well.

To introduce a change in the translational states, it is worth noting that the aircraft velocity in the inertial reference frame can be computed as follows:

$$v_I = R_b^I v_b = \bar{u}\begin{pmatrix}\cos\gamma\cos\chi\\ \cos\gamma\sin\chi\\ -\sin\gamma\end{pmatrix}, \tag{3}$$

where $\bar{u}$, γ, and χ represent the vehicle's velocity magnitude, the flight path angle, and the heading angle, respectively. Also, R_b^I denotes the transformation matrix from the body frame to the inertial frame. As a result, the system states involved in the outer and the inner loops are defined, respectively, as follows:

$$x_1 = \left[\bar{u}, \gamma, \chi\right]^T = \begin{bmatrix}\bar{u}\\ \xi\end{bmatrix}, \tag{4}$$

$$x_2 = \left[\dot{\phi}, \dot{\theta}, \dot{\psi}\right]^T = \begin{bmatrix}\dot{\Phi}\\ \bar{x}_2\end{bmatrix}, \tag{5}$$

where $\xi = \left[\gamma, \chi\right]^T$. In addition, $\Phi = [\phi, \theta, \psi]^T$ represents the Euler angles and $\bar{x}_2 = \left[\dot{\theta}, \dot{\psi}\right]^T$. Considering the fact that the aerial robot includes four independent control inputs, only four degrees of freedom of the system can be directly controlled. Thus, here, $\bar{u}$ and x_2 are chosen as the primary system states to be controlled, and ξ is controlled indirectly using a backstepping scheme.

Accordingly, concerning the translational dynamics, $\dot{\bar{u}}$ could be determined using (2). Besides, having the following equations,

$$\gamma = \theta - \alpha, \tag{6}$$

$$\chi = \psi + \beta, \tag{7}$$

where α and β represent, respectively, the angle of attack and the sideslip angle, it can be obtained that:

$$\dot{\xi} = \begin{bmatrix}\dot{\gamma}\\ \dot{\chi}\end{bmatrix} = \begin{bmatrix}\dot{\theta}\\ \dot{\psi}\end{bmatrix} + \Delta_1(\mathcal{X}, n) = \bar{x}_2 + \Delta_1(\mathcal{X}, n), \tag{8}$$

where $\mathcal{X} = \left[v_b^T, \omega^T, \Phi^T\right]^T$. Also, n and $\Delta_1(\mathcal{X}, n)$ represent, respectively, bounded measurement noises and an uncertain term, which is a function of system states and measurement noises. It is worth noting that, using such a formulation, the time derivative of α and β is included in $\Delta_1(\mathcal{X}, n)$, and thus, there is no need to compute them.

On the other hand, regarding the rotational dynamics, the time derivative of the Euler angles can be determined using the kinematic equations as follows (Stevens, Lewis, & Johnson, 2015):

$$x_2 = \begin{pmatrix}1 & \sin\phi\tan\theta & \cos\phi\tan\theta\\ 0 & \cos\phi & \sin\phi\\ 0 & \sin\phi\sec\theta & \cos\phi\sec\theta\end{pmatrix}\omega, \tag{9}$$

where $\omega = [P, Q, R]^T$ denotes the angular velocity of the vehicle in the body coordinate system. By combining (9) and (1), the rotational dynamic model of the air vehicle can be obtained as $\dot{x}_2 = \bar{F}_r(\mathcal{X}, u)$ with $\bar{F}_r$ denoting a nonlinear function.

Assumption 1. The rotational dynamic model of the aerial robot can be formulated as follows:

$$\dot{x}_2 = F(\mathcal{X}) + B(\mathcal{X})u + \Delta_2(\mathcal{X}, u) + \bar{d}_2(t), \tag{10}$$

where Δ_2 and $\bar{d}_2(t)$ represent the lumped uncertainty (consisting of the effects of actuator faults, unmodeled dynamics, and parameter uncertainties) and external disturbances, respectively. Further, $F(\mathcal{X})$ and $B(\mathcal{X})$ denote the nominal part of the dynamic model, which is assumed to be initially available. In the current study, the nominal model of the system is obtained using the frequency-domain system identification method (Emami & Banazadeh, 2016).

Remark 1. The introduced model (10) is a commonly-used, generic, nonlinear model for the rotational part of an aircraft (Emami et al., 2022) that is valid in the case of an aerial vehicle with affine dynamics.

According to the introduced formulation, in the following section, the control system will be developed as a two-loop structure, where both loops are designed using a composite learning adaptive neural framework.

3. Control design process

3.1. Guidance loop

3.1.1. Reference heading and flight path angles

The outer control loop, which is typically known as the guidance loop, attempts to transform the reference trajectory into a desired velocity and attitude. To this end, the desired velocity in the inertial reference frame can be defined as

$$v_d = \dot{r}_d - k_X e_r - k_I \int_0^t e_r d\tau, \tag{11}$$

with k_X and k_I denoting positive-definite matrices. It is easy to show that $e_r \to 0$ if $v \to v_d$. Subsequently, it is possible to define the following parameters:

$$v_d =: \bar{u}_d \begin{pmatrix} \cos\gamma_d \cos\chi_d \\ \cos\gamma_d \sin\chi_d \\ -\sin\gamma_d \end{pmatrix}. \tag{12}$$

Here, γ_d, χ_d, and $\bar{u}_d$ denote the desired flight path angle, the desired heading angle, and the desired velocity magnitude, respectively. Consequently, it is obtained that:

$$\gamma_d = \arcsin\left(\frac{-v_{d_z}}{\bar{u}_d}\right), \tag{13}$$

$$\chi_d = \arctan\left(\frac{v_{d_y}}{v_{d_x}}\right), \tag{14}$$

$$\bar{u}_d = \sqrt{v_{d_x}^2 + v_{d_y}^2 + v_{d_z}^2}. \tag{15}$$

Now, $\bar{u}_d$ is sent to a distinct velocity control loop in which the throttle setting is employed as the control input. Due to the insignificant changes in $\bar{u}_d$ in a typical trajectory tracking problem, a simple controller can be utilized to control the velocity magnitude. In the current research, after obtaining an equivalent linear model of the velocity subsystem using the system identification approach, an LQG controller is designed and employed, where the computed control command is equally distributed on all the available electric motors.

In addition, by defining $e_\xi = \xi - \xi_d$ and using (8), we have:

$$\dot{e}_\xi = \bar{x}_2 + \Delta_1 - \dot{\xi}_d, \tag{16}$$

where $\dot{\xi}_d$ could be computed by differentiating (13)–(14).

3.1.2. NN-based uncertainty estimation

Subsequently, we attempt to estimate Δ_1 using a NN. As the uncertain terms considered in this work (i.e., Δ_1 and Δ_2) are nonlinear functions of *current* system states and inputs, they can be estimated using feedforward NNs as $\hat{\Delta}_1(\mathcal{X}) = \hat{W}_1^T \mu_1(\mathcal{X})$, where $\hat{W}_1$ and $\mu_1(\mathcal{X})$ denote unknown output weights and an appropriate basis function matrix. This is a generic formulation, which can be employed for a NN with arbitrary hidden layers considered in $\mu_1(\mathcal{X})$. Similar to an Extreme Learning Machine (ELM), single-hidden layer NNs (with radial basis functions in their hidden layer) are used in this work, where the parameters of the hidden layer $\mu_1(\mathcal{X})$ are chosen as random constants, and only the output weight matrix $\hat{W}_1$ is updated at each step. Considering radial basis functions as the activation function of the hidden layer, the adjustable parameters of each function that are chosen randomly include the center and the width of each Gaussian function. Along with a simpler training algorithm with less computational complexity, such an approach can provide better generalization performance compared to traditional feedforward NNs (Huang, Zhu, & Siew, 2006), while satisfying the universal approximation property (Liang, Huang, Saratchandran, & Sundararajan, 2006). This architecture has been utilized in this research to estimate uncertain dynamics in both the guidance and control loops. Accordingly, using a sufficient number of hidden nodes, it is obtained that:

$$\Delta_1(\mathcal{X}, n) = {W_1^*}^T \mu_1(\mathcal{X}) + \epsilon_1(\mathcal{X}, n), \tag{17}$$

where W_1^* and ϵ_1 represent the unknown optimal weights and the bounded estimation error of the NN. Thus, we have $|\epsilon_1(\mathcal{X})| \preceq \varepsilon_{1M}$, where ε_{1M} denotes an unknown constant vector and $\preceq$ is used for the element-wise inequality. Notice that, in this paper, the absolute value function (as well as the signum function) of a vector is applied to each element of the vector.

3.1.3. Disturbance observer

Now, to compensate for the estimation error ϵ_1 (which also includes the measurement noises that could not be captured by the NN), a disturbance observer would be employed in the guidance loop to estimate an upper bound for ϵ_1. More precisely, by defining $D_{1M}^* = \varepsilon_{1M}$, it is possible to introduce a disturbance observer to estimate D_{1M}^* using the tracking error of the guidance loop.

As discussed earlier, as an effective approach to enhance the learning process, a state observer is also defined as follows:

$$\dot{\hat{\xi}} = \bar{x}_2 + \hat{\Delta}_1 + \hat{D}_{1M} \otimes \text{sign}\left(\mathcal{E}_\xi\right) - \kappa_1 e_{s_1}, \tag{18}$$

where $\otimes$ denotes the element-wise multiplication, and

$$e_{s_1} = \hat{\xi} - \xi, \tag{19}$$

$$\mathcal{E}_\xi = e_\xi - k_{s_1} e_{s_1}, \tag{20}$$

with k_{s_1} and κ_1 denoting positive-definite matrices. Indeed, in the following, in addition to the tracking error e_ξ, the estimation error e_{s_1} is also incorporated into the design process to improve learning efficiency. In the current study, such a *composite* learning scheme (Xu et al., 2014) is employed in both the guidance and control loops to provide a resilient flight management system.

Consequently, the desired attitude command is formulated as

$$\bar{x}_{2_d} = \dot{\xi}_d - k_1 e_\xi - \hat{W}_1^T \mu_1(\mathcal{X}) - \hat{D}_{1M} \otimes \text{sign}\left(\mathcal{E}_\xi\right), \tag{21}$$

and the following updating rules are employed.

$$\dot{\hat{W}}_1 = \Gamma_1 \mu_1(\mathcal{X}) \mathcal{E}_\xi^T, \tag{22}$$

$$\dot{\hat{D}}_{1M} = k_{D_1} \left|\mathcal{E}_\xi\right|, \tag{23}$$

where $\hat{D}_{1M}$ represents the estimation of D_{1M}^*. Also, k_{D_1} and Γ_1 denote positive definite matrices.

Theorem 1. *Using the attitude command (21) and the updating rules (22)–(23), the guidance loop would be asymptotically stable, thereby guaranteeing the convergence of both the tracking error e_ξ and the estimation error e_{s_1} to zero.*

Proof. See Appendix A.

Remark 2. The use of the signum function in the state observer (18) and the control command (21) may lead to the undesirable chattering phenomenon, which is a common issue in discontinuous control methods (Patre, MacKunis, Kaiser, & Dixon, 2008). As an effective approach to overcome such an issue, it is possible to replace the signum function in (18) and (21) with the hyperbolic tangent function and the absolute value function $|\lambda|$ in (23) with $\lambda \tanh \lambda$, while the asymptotic stability would be reduced to the bounded stability. More precisely, using this substitution and considering the inequality

$$0 \le |\lambda| - \lambda \tanh\left(\frac{\lambda}{\epsilon_\lambda}\right) \le 0.2785\epsilon_\lambda$$

for any $\epsilon_\lambda > 0$ and $\lambda \in \mathbb{R}$ (Polycarpou, 1996), the bounded tracking error in the guidance loop can be guaranteed (Zou & Zheng, 2015). Another beneficial approach, which does not violate the asymptotic stability of the guidance system, has been given in Li, Hou, Liang, and Jiao (2020) and Zuo and Wang (2014). Specifically, the signum function of λ can be replaced with $\lambda / \left(\sqrt{\lambda^2 + \nu^2}\right)$, where $\nu(t)$ denotes a vanishing positive function satisfying $\int_0^\infty \nu^2(t)dt < \infty$.

Remark 3. Another concern with the given updating rules (22)–(23) is the possibility of parameter drift (in the absence of a persistent excitation) in real applications due to the requirement for a discrete-time implementation of the introduced design. As mentioned previously, different modifications such as the σ-modification or the e-modification techniques (Lungu, 2020; Rysdyk & Calise, 2005) could be incorporated into the above-mentioned updating rules, while, again, the asymptotic stability of the system is reduced to a bounded tracking error.

It is worth mentioning that the above-mentioned techniques do not solve the fundamental problem of the adaptive updating rules in the absence of a persistent excitation that is the lack of information-rich data in the learning process. As an effective approach to overcome this issue, in this work, a composite learning scheme has been adopted in which the updating rules employ a composite error function including both the tracking error of the system and the estimation error of a state observer. Accordingly, by incorporating such a composite error function in the updating rules of both the NN and DO, more information about the system is involved in updating the unknown coefficients of the NN and DO. Also, even in the lack of the PE condition, we can satisfactorily estimate an upper bound for the entire uncertain terms in the model using the introduced DO. More precisely, the NN is an adaptive term, while the DO can be considered a robust term to compensate for the residual uncertain dynamics that have not been compensated by the NN. Thus, the more information on system dynamics we have (by using appropriate excitations or involving more informative error functions such as the introduced composite learning method), the greater the contribution of the NN in the estimation of uncertain dynamics. The DO can compensate for the residual terms that have not been captured by the NN, while the more the DO's contribution to the estimation of uncertain dynamics, the more conservative the control command becomes.

Remark 4. An adaptive trajectory tracking algorithm has been developed in Sonneveldt, van Oort, Chu, and Mulder (2009), where, in a somewhat similar manner to the aforementioned formulation, the desired trajectory is transformed to the desired flight path angle and the heading angle in the guidance loop. However, the entire closed-loop system in Sonneveldt et al. (2009) consists of a complicated structure with four control loops, while asymptotic stability can be ensured only in the presence of parametric uncertainties. Alternatively, the novel, simple, and generic formulation of the guidance problem introduced in this paper can be effectively employed in real applications with guaranteed asymptotic stability in the presence of nonparametric uncertainties and unmodeled dynamics, while there is no need to directly control the angle of attack and the sideslip angle in this formulation.

Finally, regarding the roll angle, although it does not explicitly appear in the above-mentioned equations, the required centrifugal force to provide the desired heading angle leads to a constraint on the roll angle (Ducard, 2009; Emami & Banazadeh, 2019). More precisely, considering the ratio between the required centrifugal force and the desired vertical force, we have:

$$\tan\phi_d = \frac{\dot{\chi}_d v_{d_{xy}}}{g - \dot{v}_{d_z}}, \tag{24}$$

where $v_{d_{xy}} = \sqrt{v_{d_x}^2 + v_{d_y}^2}$ and g denotes the gravity acceleration. It is notable that, practically, it would be more efficient to replace $\dot{\chi}_d$ in (24) with $\dot{\psi}_d$ to eliminate the undesirable effects of fluctuations in the sideslip angle from the roll command. Subsequently, the desired *roll rate* can be simply obtained using (24) through a proportional or Proportional–Derivative (PD) controller. Thus, the desired attitude can be finally constructed as $x_{2_d} = \begin{bmatrix} \dot{\phi}_d & \bar{x}_{2_d}^T \end{bmatrix}^T$.

3.2. Control loop

After determining the desired attitude, the inner control loop attempts to track the reference attitude using the available control inputs, i.e., the elevator, the aileron, and the rudder deflections (as mentioned earlier, the throttle setting is employed as the primary system input in the velocity control loop).

Considering the dynamic model (10), the uncertain term $\Delta_2(\mathcal{X}, u)$ can be identified using a feedforward NN as $\Delta_2(\mathcal{X}, u) = {W_2}^{*T}\mu_2(\mathcal{X}, u) + \epsilon(\mathcal{X}, u)$, where its estimation is derived as

$$\hat{\Delta}_2(\mathcal{X}, u) = \hat{W}_2^T \mu_2(\mathcal{X}, u). \tag{25}$$

Subsequently, by defining $d_2(t) = \bar{d}_2(t) + \epsilon(\mathcal{X}, u)$ and assuming that external disturbances are bounded, we have

$$|d_2(t)| \preceq D_{2M}^*, \tag{26}$$

where D_{2M}^* represents an unknown constant vector, and $\hat{D}_{2M}$ denotes its estimation (Fu et al., 2018). Accordingly, using the definition of $e = x_2 - x_{2_d}$ and the following state observer,

$$\dot{\hat{x}}_2 = F(\mathcal{X}) + B(\mathcal{X})u + \hat{\Delta}_2 + \hat{D}_{2M} \otimes \operatorname{sign}(\mathcal{E}) - \kappa_2 e_{s_2}, \tag{27}$$

where,

$$e_{s_2} = \hat{x}_2 - x_2, \tag{28}$$

$$\mathcal{E} = e - k_{s_2} e_{s_2}, \tag{29}$$

the control command can be constructed as follows:

$$u = B(\mathcal{X})^{-1}\left(\dot{x}_{2_d} - F(\mathcal{X}) - k_2 e - \hat{\Delta}_2 - \hat{D}_{2M} \otimes \operatorname{sign}(\mathcal{E})\right), \tag{30}$$

where k_2, k_{s_2}, and κ_2 denote positive-definite matrices, and the updating rules of the NN and the disturbance observer are obtained as:

$$\dot{\hat{W}}_2 = \Gamma_2 \mu_2(\mathcal{X}, u)\mathcal{E}^T, \tag{31}$$

$$\dot{\hat{D}}_{2M} = k_{D_2} |\mathcal{E}|. \tag{32}$$

Theorem 2. *Using the control command (30) and the updating rules (31)–(32), the (inner) control loop is asymptotically stable under Assumption 1.*

Proof. See Appendix A.

Remark 5. Unlike (Yu, Zhang, Jiang, Su et al., 2020), here, there is no need to make an assumption on the boundedness of the time derivative of $d_2(t)$ to ensure closed-loop stability.

The overall view of the proposed control scheme is shown in Fig. 1.a, while a detailed schematic view of the closed-loop system is illustrated in Fig. 1.b. In the following section, the performance of the developed neuroadaptive guidance and control system would be carefully evaluated in different flight scenarios.

4. Simulation results

4.1. Simulator and controller description

A detailed nonlinear simulation of a 25 percent dynamically similar model of a newly designed electric aerial robot that benefits from distributed propulsion system (as presented in Fig. 2) is employed in this research to evaluate the performance of the designed guidance and control system. To be more specific, it is a *coupled* 6 degrees of freedom dynamic model consisting of a detailed nonlinear model of aerodynamic and propulsive forces and moments. The details of the forces and moments acting on the aerial robot are given in Appendix B. Also, the aerodynamic coefficients of the aircraft are obtained at first by the numerical rules according to the aircraft geometry, and subsequently, they are validated and refined by the finite-element

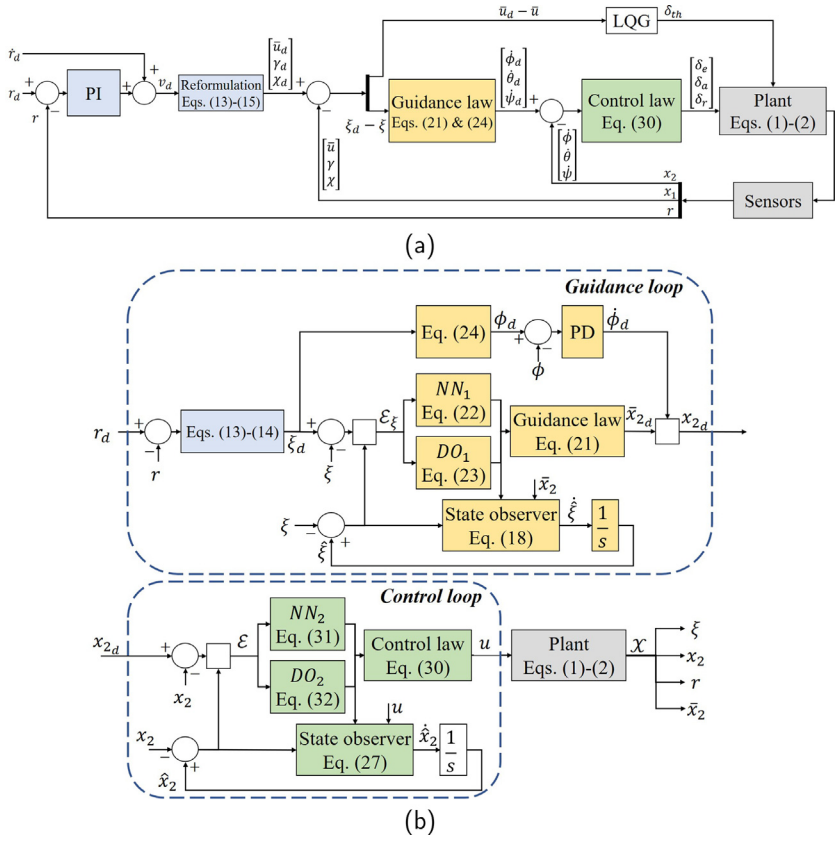

Fig. 1. (a) Overall view of proposed control design, (b) Detailed schematic view of the closed-loop system.

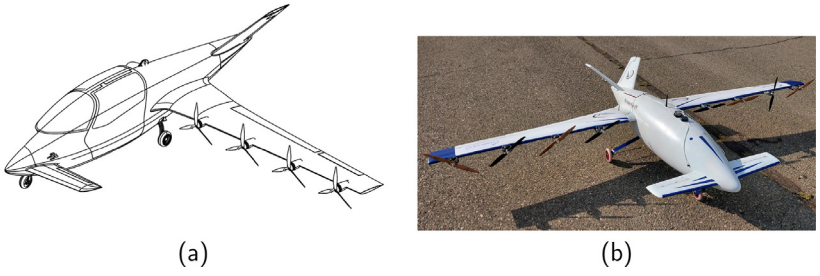

Fig. 2. (a) Schematic view of the aerial robot, (b) Prototype built for flight tests.

analysis (in OpenVSP developed by NASA) (see Fig. 3) and finally, using the information extracted from several real flight experiments. The simulations are performed in MATLAB/Simulink. The numerical values of the aircraft parameters are given in Table 1.

Remark 6. It is worth mentioning that, to evaluate the controller's capability to deal with highly nonlinear uncertainties, in the following, it is assumed that the nominal model of the aerial robot, which is employed in the control design process, is a simple linearized model of the aerial robot. Accordingly, the controller should learn all the nonlinear terms in the model using the proposed NNs and DOs. Subsequently, the computed control commands would be applied to the above-mentioned nonlinear model of the aerial robot.

To demonstrate the outstanding performance of the proposed control system, the nominal model of the aerial robot, which is employed to compute the control command u, i.e., $F(\mathcal{X})$ and $B(\mathcal{X})$ in (30), is simply derived using the linear frequency-domain system identification. Thus, all the nonlinear terms in the dynamic model of the air vehicle are included in $\Delta_2(\mathcal{X}, u)$, which should be compensated by the introduced combined NN and DO scheme. Accordingly, the nominal dynamic model of the system is obtained as a linear state-space model for both the longitudinal and lateral-directional dynamics.

Table 1
Numerical values of the aircraft parameters.

Parameters	Description	Value
m	mass	16 kg
$[I_{xx}, I_{yy}, I_{zz}]$	Moment of inertia	$[1.08, 4.12, 5.06]$ kg m^2
S	Wing area	0.72 m^2
b	Wing span	2.95 m
c	Mean chord length	0.24 m

Remark 7. Using the introduced formulation (10), even if the obtained $B(\mathcal{X})$ is not invertible, assuming that the dynamic system is controllable, it is possible to divide the obtained $B(\mathcal{X})$ into an invertible matrix to be used in (30) and a residual part, which is included in the uncertain term $\Delta_2(\mathcal{X}, u)$.

Besides, the controller's parameters are chosen as listed in Table 2. Concerning the NNs, Radial Basis Function (RBF) NNs with a single

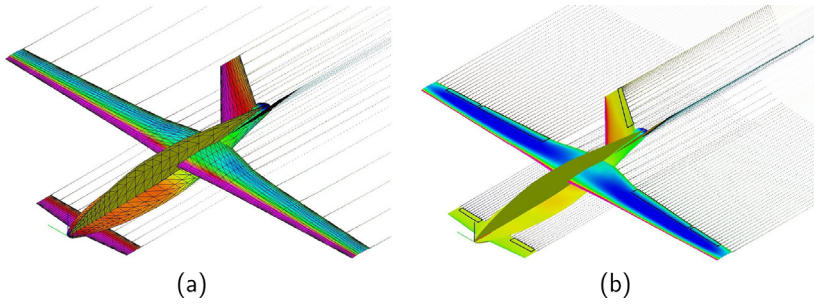

Fig. 3. The finite-element analysis result, (a) Aircraft without control surfaces (to determine stability derivatives), (b) Aircraft with control surfaces (to determine control derivatives).

Table 2
Numerical values of the controller's parameters.

Parameters	Value	Parameter	Value
k_X	diag [0.5, 0.5, 1]	k_1	diag [0.2, 0.1]
k_I	0.02	k_2	6
Γ_1	0.15	Γ_2	30
k_{D_1}	diag [0.006, 0.003]	k_{D_2}	diag [0.48, 0.4, 0.4]
κ_1	10	κ_2	25
k_{s_1}	5	k_{s_2}	0.5

hidden layer are used in both the guidance and control loops, where the hidden layer of the network consists of 30 neurons with a random center and width in the range of $[-1, 1]$ and $[0.2, 2.2]$, respectively. In addition, the system states, which are used as the network inputs, are chosen as $\mathcal{X} = \left[v_b^T, \omega^T, \phi, \theta, \psi\right]^T$, while they are normalized before entering the network. In the following, three different flight scenarios are considered to evaluate the effectiveness of the proposed guidance and control method under different flight conditions.

In this regard, the desired trajectory is defined for the air vehicle as follows:

$$y_{Id} = A\left(1 - \cos(\varpi_y x_{Id})\right), \tag{33}$$

$$z_{Id} = \frac{T_z}{\pi}\left(1 - \cos\left(\frac{2\pi t}{T_z}\right)\right), \tag{34}$$

where $A = 150$ m, $\varpi_y = \frac{2\pi}{1000}$ rad/m, and $T_z = 50$ s. This is a complex trajectory in the 3D environment.

4.2. Closed-loop performance

4.2.1. Ideal flight conditions

Now, the performance of the closed-loop system is first evaluated under ideal conditions. Accordingly, the aircraft trajectory would be obtained as shown in Fig. 4. As seen, the aerial robot could satisfactorily follow such a complex trajectory. The control commands applied to the vehicle are also shown in Fig. 5.a. In addition, the estimated and real values of the system states involved in the inner control loop are illustrated in Fig. 7. As can be seen, all the control commands are feasible, while the introduced observer could satisfactorily estimate the Euler angles' rate.

4.2.2. Robustness against the wind, uncertainty, and measurement noises

Subsequently, to evaluate the robustness of the proposed control system, severe Dryden wind turbulence is applied to the aircraft. In addition, up to 20 percent *random uncertainty* is considered in almost all of the aircraft's primary parameters including the total mass, the moment of inertia, and aerodynamic coefficients. Uncertain dynamics (N_{th}) in the engines' model (see Appendix B) and about 10% measurement noises in all the measured states are also considered in this scenario. As a result, the air vehicle's trajectory and the system inputs are obtained as shown in Figs. 4 and 5.b, respectively. As seen, the aerial robot can follow the desired trajectory even in the presence of severe external disturbances and measurement noises. Further, as can be observed in Fig. 7.b, the state observer could estimate the system states, satisfactorily.

4.2.3. Faulty conditions

In the final scenario, severe actuator faults are applied to all three control surfaces, i.e. the elevator, the aileron, and the rudder actuators in both the multiplicative and additive manners. More specifically, we have:

$$\text{Elevator: } G_e = 0.7, \quad B_e = 0.2 \text{ deg}, \quad \text{for } t > 20 \text{ s}, \tag{35}$$

$$\text{Aileron: } G_a = 0.6, \quad B_a = 0.3 \text{ deg}, \quad \text{for } t > 35 \text{ s}, \tag{36}$$

$$\text{Rudder: } G_r = 0.8, \quad B_r = -0.1 \text{ deg}, \quad \text{for } t > 25 \text{ s}, \tag{37}$$

where G_i and B_i denote the multiplicative and additive faults, respectively. Notice that, since no redundant actuator is considered in the aerial robot, the proposed controller does not necessarily have to be effective in the presence of a complete loss of effectiveness or the lock-in-place fault. Again, up to 20 percent uncertainty is applied to model parameters. Significant external disturbances are also applied to the total forces and moments as follows:

$$d_F = 0.5\begin{bmatrix} \sin\left(\frac{2\pi t}{10}\right) \\ \sin\left(\frac{2\pi t}{12}\right) \\ \sin\left(\frac{2\pi t}{8}\right) \end{bmatrix}, \quad d_M = 0.1\begin{bmatrix} \sin\left(\frac{2\pi t}{9} + \frac{\pi}{5}\right) \\ \sin\left(\frac{2\pi t}{3} + \frac{\pi}{4}\right) \\ \sin\left(\frac{2\pi t}{6} + \frac{\pi}{7}\right) \end{bmatrix}. \tag{38}$$

The introduced sinusoidal signals can be considered a representation of real atmospheric disturbances such as microburst wind shears (Pourtakdoust, Kiani, & Hassanpour, 2011). The uncertain dynamics in the engine model are considered in the model as well, while the measurement noises are not included in this scenario to better illustrate the computed control commands in the presence of actuator faults. Therefore, the air vehicle's trajectory, as well as the system inputs, is demonstrated, respectively, in Figs. 4 and 5.c. As observed, again, the aerial vehicle is capable of following the desired trajectory under severe actuator faults and external disturbances.

Besides, by defining the following two criteria, i.e. the Root Mean Square Error (RMSE) and the Control Effort (CE), the performance of the closed-loop system under different flight conditions can be better evaluated and compared.

$$RMSE = \sqrt{\frac{1}{T}\int_0^T e_r^T e_r \; dt}, \tag{39}$$

$$CE = \sqrt{\frac{1}{T}\int_0^T u^T u \; dt}. \tag{40}$$

To this end, the obtained tracking error, control effort, and the estimation error of the introduced state observer (in the inner control loop) denoted by RMSE_O are given in Table 3 for different flight conditions. As can be observed, the average tracking error is less than 1 m in all the scenarios, while the control effort remains acceptable. Accordingly, the

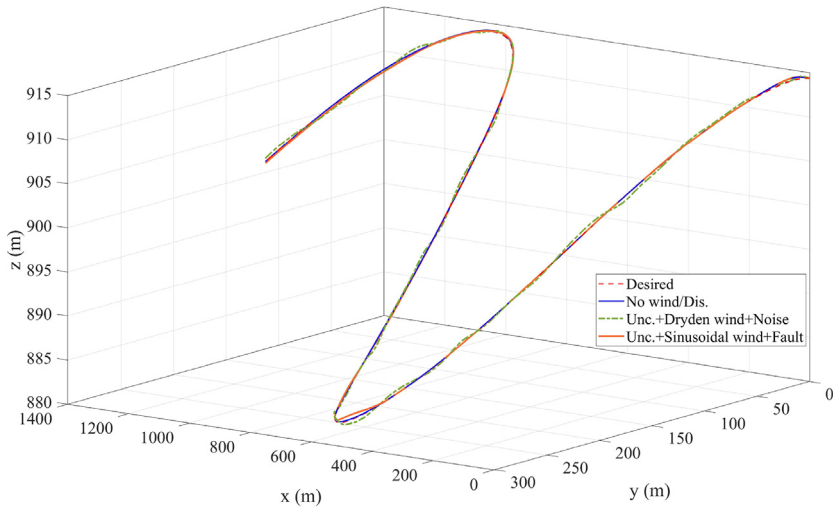

Fig. 4. Aerial vehicle trajectory in different flight conditions.

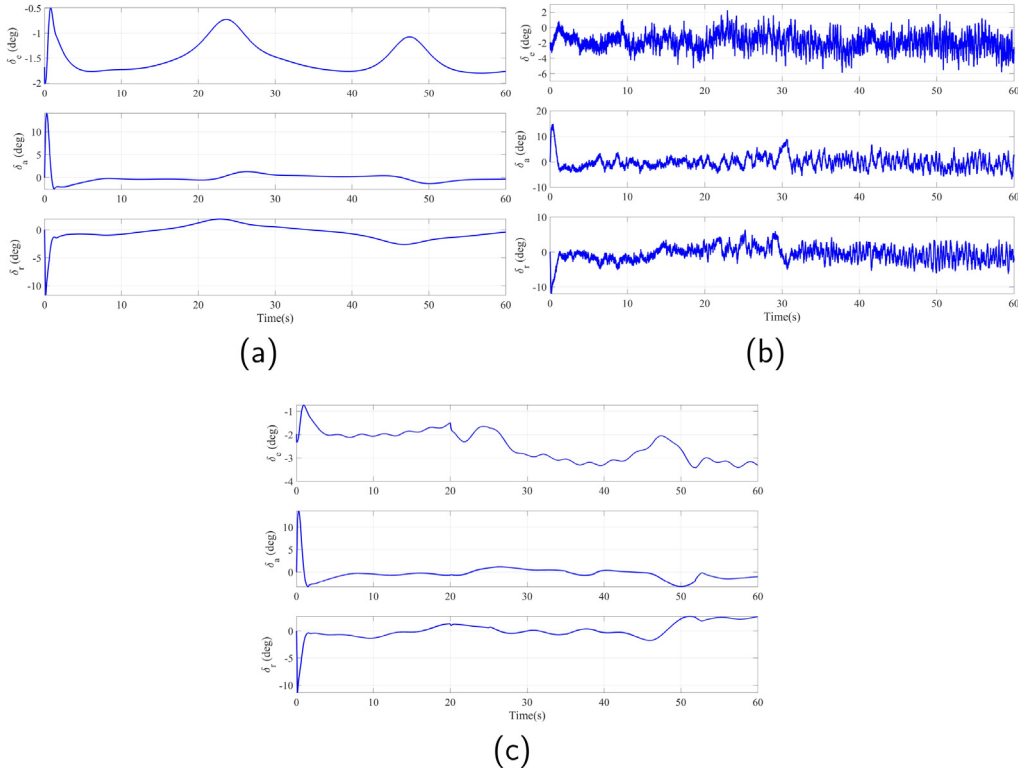

Fig. 5. Aerial vehicle inputs in different flight conditions, (a) Ideal condition, (b) Considering Dryden wind model, model uncertainties, and measurement noises, (c) Considering Sinusoidal wind model, model uncertainties, and actuator faults.

Table 3
The obtained results in different flight scenarios.

Scenario	RMSE (m)	CE (deg)	$RMSE_O$ (rad/s)
Ideal	0.465	2.04	0.0034
Unc. + Dryden wind + Noise	0.85	3.6	0.0185
Unc. + Sinusoidal wind + Fault	0.66	2.35	0.0063

proposed control system can result in a resilient and reliable trajectory tracking control scheme in the presence of significant model uncertainties, atmospheric disturbance, measurement noises, and actuator faults.

4.3. Estimation performance of the proposed combined NN and DO

As mentioned above, actuator faults including both multiplicative and additive cases can be estimated and compensated by the introduced scheme. Besides, regarding the saturation of control surfaces, this phenomenon has been considered in flight simulations, and the proposed control system can satisfactorily deal with it. However, the saturation issue is not the main subject of this work, and there are well-known approaches (like the employment of a modified tracking error in the learning rule to compensate for the effect of different actuator constraints Emami et al., 2022) that can be integrated with the proposed control system in this work.

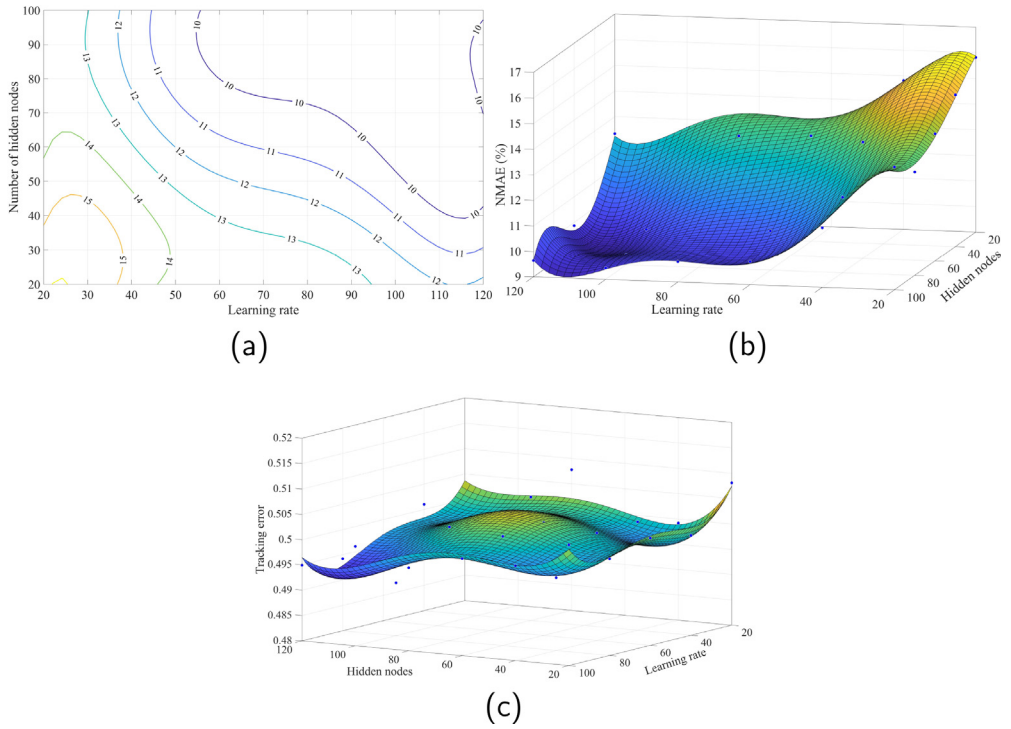

Fig. 6. Estimation performance of the proposed combined NN+DO under different values of the learning rate and hidden nodes, (a) Estimation error contours, (b) Estimation error surface, (c) Trajectory tracking error.

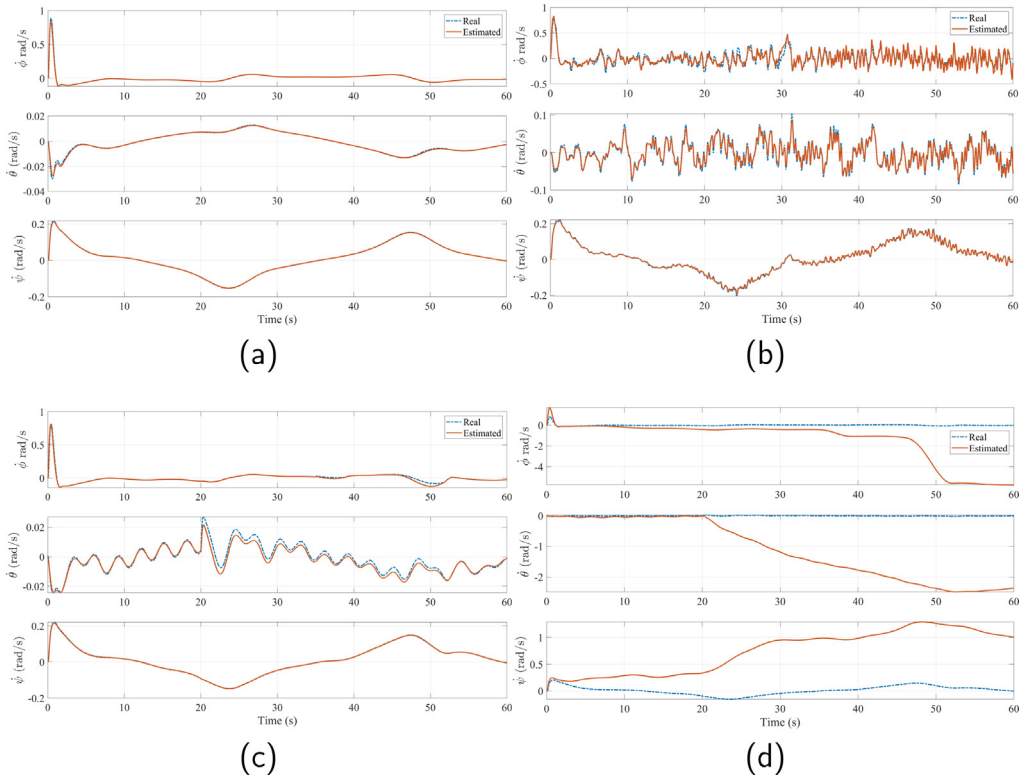

Fig. 7. Estimated versus real states in the inner control loop, (a) Ideal condition, (b) Considering Dryden wind model, model uncertainties, and measurement noises, (c) Considering Sinusoidal wind model, model uncertainties, and actuator faults, (d) in the absence of the proposed composite learning scheme.

In addition, concerning the estimation accuracy of the combined NN and DO employing the composite learning method, the Normalized Mean Absolute Error (NMAE) of the estimation in the inner control loop can be defined as follows:

$$Unc_T = \Delta_2(\mathcal{X}, u) + \bar{d}_2(t) = \dot{x}_2 - F(\mathcal{X}) - B(\mathcal{X})u, \tag{41}$$

$$Unc_E = \hat{W}_2^T \mu_2(\mathcal{X}, u) + \hat{D}_{2M} \otimes \text{sign}(\mathcal{E}), \tag{42}$$

$$NMAE = \frac{\int_0^T |Unc_T - Unc_E|\, dt}{\int_0^T |Unc_T|\, dt} \times 100\%. \tag{43}$$

Here, Unc_T and Unc_E denote, respectively, the real and estimated uncertain dynamics considered in the dynamic model. As can be seen in Fig. 6.a and b, by increasing the learning rate (Γ_2) and the number of hidden nodes in the hidden layer of the NN, the estimation error generally decreases (while using a very high learning rate can cause numerical issues). Accordingly, an estimation error of less than 10% can be obtained even in the presence of severe internal and external uncertain dynamics.

On the other hand, because the identified dynamic model has been utilized in a closed-loop system, trajectory tracking performance, which is the main purpose of this scheme, is satisfactory even by employing lower values of the learning rate and fewer hidden nodes (see Fig. 6.c). Consequently, by employing the NN-based estimation combined with DO, the proposed scheme could effectively benefit from the capabilities of both schemes. More precisely, the DO brings the uncertain dynamics into the domain of attraction of the NN, and then, the NN compensates for the state-dependent uncertainties. Accordingly, the DO complements the role of the NN in the closed-loop system, thereby satisfactorily eliminating the requirement for high learning rates. In other words, even if the NN is removed from the design, the closed-loop system remains stable, while the DO should compensate for the entire uncertain dynamics, resulting in a conservative design with a possible chattering phenomenon due to the requirement for high gains in the estimation process.

4.4. Composite learning contribution evaluation

Finally, to demonstrate the significant importance of the proposed composite learning approach, the real and the estimated system states (i.e. the change rate of Euler angles) computed using the state observer (27) both in the presence and the absence of the composite learning method (considering the above-mentioned external disturbances, actuator faults, and model uncertainties), are depicted in Fig. 7.c and d, respectively (to eliminate the composite learning scheme from the control loop, it is sufficient to set $k_{s_2} = \kappa_2 = 0$). As seen, without the composite learning algorithm, the presence of actuator faults, atmospheric disturbances, and/or model uncertainties would seriously deteriorate the estimation performance (for example, the estimation of the $\dot{\theta}$ becomes significantly worsen after $t = 20$ s, which is the start time of the elevator fault). Thus, in the absence of the proposed composite learning scheme, the control command is computed based on inaccurate information about the system dynamics. This is a problematic issue, which can lead to improper commands (or even closed-loop instability) in the presence of considerable change in the system dynamics. On the other hand, using the proposed control system consisting of the introduced composite learning method, the observer can effectively estimate the system states under severe internal and external disturbances. As a result, there is no requirement for an RLS-based identification scheme (as recommended in Abbaspour et al., 2017; Nguyen et al., 2008), which brings significant challenges to the analysis of closed-loop stability. Consequently, the introduced guidance and control strategy can be employed as a reliable flight management system for different types of fixed-wing aerial robots in the presence of significant uncertain dynamics, external disturbances, actuator faults, and measurement noises.

5. Conclusions

An adaptive neural guidance and control system was introduced in this paper. By employing a composite learning method, which incorporates both the tracking and estimation errors into the learning process, an effective learning algorithm was introduced to train a neural network as well as a disturbance observer to compensate for the effects of unmodeled dynamics and external disturbances, respectively. The disturbance observer is also responsible for compensating the neural network's estimation error. Such an approach was employed in both the guidance and control systems to provide an entirely adaptive flight management system. Finally, the proposed control system was applied to a realistic dynamic model of an electric aircraft, which was validated based on real data and flight experiments. According to the obtained simulation results, using the developed guidance and control method, the aircraft is capable of tracking the desired trajectory in a 3D environment under different types of external disturbances, model uncertainties, actuator faults, and measurement noises. In future work, the authors will attempt to extend the introduced control method to a space vehicle to develop a resilient control system for a satellite considering different types of internal and external disturbances. In addition, although the proposed control scheme could satisfactorily deal with measurement noises and actuator dynamics in provided flight simulations, the consideration of actuator dynamics in the *control design process* to theoretically ensure the closed-loop stability in the presence of different types of actuator dynamics would be an important research direction in future works.

Declaration of competing interest

The authors declare that they have no known competing financial interests or personal relationships that could have appeared to influence the work reported in this paper.

Acknowledgments

This work was supported by Iran National Science Foundation (INSF) and Iran's National Elites Foundation (INEF) grant 98027065.

Appendix A. Stability analysis

The stability of the guidance and control loops can be separately analyzed considering the *time-scale decomposition assumption*. More precisely, it is worth noting that the inner control loop (i.e. the attitude control loop) is significantly faster than the outer loop, which corresponds to the position control. Thus, using the time-scale decomposition and by designing an appropriate attitude control loop that can ensure the asymptotic tracking of the attitude commands, in the stability analysis of the outer loop (i.e. the guidance loop), it could be assumed that $\bar{x}_{1_d} \approx \bar{x}_1$.

In addition, the stability of both loops can be proved in a similar way. Thus, here, we address only the stability analysis of the (inner) control loop. To this end, a Lyapunov function can now be defined as given below.

$$V_2 = \frac{1}{2} e^T e + \frac{1}{2} e_{s_2}^T k_{s_2} e_{s_2} + \frac{1}{2} tr\left(\tilde{W}_2^T \Gamma_2^{-1} \tilde{W}_2\right) + \frac{1}{2} \tilde{D}_{2M}^T k_{D_2}^{-1} \tilde{D}_{2M}, \tag{A.1}$$

where,

$$\tilde{W}_2 = \hat{W}_2 - W_2^*, \tag{A.2}$$

$$\tilde{D}_{2M} = \hat{D}_{2M} - D_{2M}^*, \tag{A.3}$$

and tr denotes the trace function. Accordingly, the time-derivative of V_2 can be obtained as

$$\begin{aligned}
\dot{V}_2 &= e^T \dot{e} + e_{s_2}^T k_{s_2} \dot{e}_{s_2} + tr\left(\tilde{W}_2^T \Gamma_2^{-1} \dot{\tilde{W}}_2\right) + \tilde{D}_{2M}^T k_{D_2}^{-1} \dot{\tilde{D}}_{2M} \\
&= e^T \left(-k_2 e - \tilde{W}_2^T \mu_2 + d_2\right) \\
&\quad + e_{s_2}^T k_{s_2} \left(-\kappa_2 e_{s_2} + \tilde{W}_2^T \mu_2 - d_2\right) - |\mathcal{E}|^T \hat{D}_{2M} \\
&\quad + tr\left(\tilde{W}_2^T \Gamma_2^{-1} \dot{\tilde{W}}_2\right) + \tilde{D}_{2M}^T k_{D_2}^{-1} \dot{\tilde{D}}_{2M} \\
&\le -e^T k_2 e - e_{s_2}^T k_{s_2} \kappa_2 e_{s_2} - \mathcal{E}^T \tilde{W}_2^T \mu_2 - |\mathcal{E}|^T \tilde{D}_{2M} \\
&\quad + tr\left(\tilde{W}_2^T \Gamma_2^{-1} \dot{\tilde{W}}_2\right) + \tilde{D}_{2M}^T k_{D_2}^{-1} \dot{\tilde{D}}_{2M}.
\end{aligned} \tag{A.4}$$

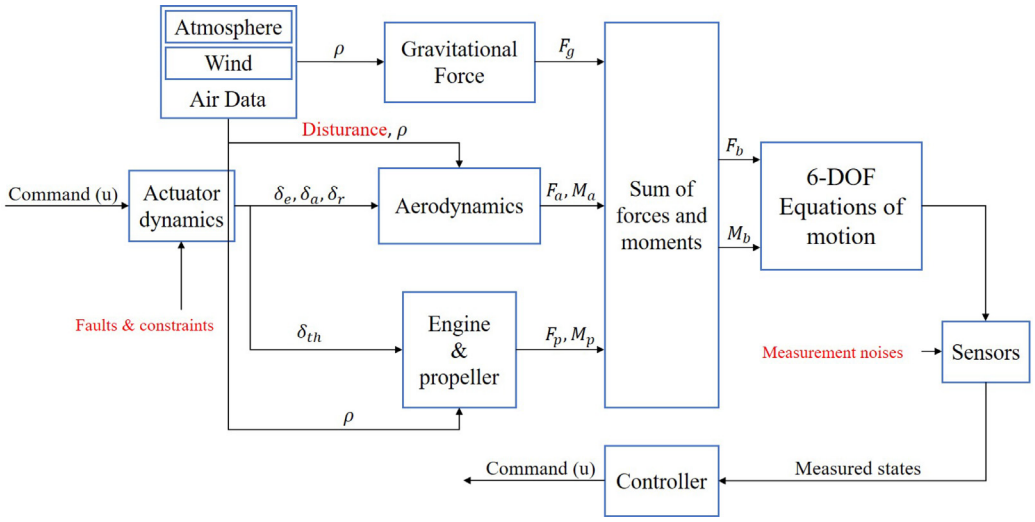

Fig. B.8. Overall structure of the proposed nonlinear flight simulator.

Consequently, using the updating rules (31)–(32), it is obtained that

$$\dot{V}_2 \leq -e^T k_2 e - e_{s_2}^T k_{s_2} \kappa_2 e_{s_2}, \tag{A.5}$$

thereby guaranteeing the asymptotic stability of the attitude control system. As a result, considering the proposed combination of the guidance and control loops, the asymptotic stability of the closed-loop system can be satisfactorily ensured in the presence of model uncertainties, unmodeled dynamics, and external disturbances.

Appendix B. Details of the aerial robot dynamic model

The overall structure of the provided flight simulator is demonstrated in Fig. B.8. In this regard, total forces and moments acting on the aerial robot, i.e., F_b and M_b in (1)–(2) can be formulated as follows (Stevens et al., 2015):

$$F_b = \begin{pmatrix} -mg\sin\theta + F_{a_x} + T \\ mg\cos\theta\sin\phi + F_{a_y} \\ mg\cos\theta\cos\phi + F_{a_z} \end{pmatrix}, \tag{B.1}$$

$$M_b = T_w^b \begin{pmatrix} \ell \\ M \\ N \end{pmatrix} + M_T, \tag{B.2}$$

where,

$$\begin{pmatrix} F_{a_x} \\ F_{a_y} \\ F_{a_z} \end{pmatrix} = T_w^b \begin{pmatrix} -D \\ Y \\ -L \end{pmatrix}, \tag{B.3}$$

with T_w^b, $[\ell, M, N]^T$, and $[-D, Y, -L]^T$ denote the transformation matrix from the wind coordinate system to the body coordinate system, aerodynamic moments, and aerodynamic forces acting on the vehicle expressed in the wind coordinate system, respectively. In addition, T and M_T represent, respectively, the thrust forces and the moments generated by thrust forces, expressed in the body coordinate system.

B.1. Aerodynamics

Concerning the aerodynamic forces and moments, we have:

$$D = \bar{q}S\left(C_{D_0} + C_{D_\alpha}\alpha + C_{D_{\delta_e}}\delta_e\right), \tag{B.4}$$

$$Y = \bar{q}S\left(C_{Y_\beta}\beta + C_{Y_p}\frac{Pb}{2v} + C_{Y_r}\frac{Rb}{2v} + C_{Y_{\delta_a}}\delta_a + C_{Y_{\delta_r}}\delta_r\right), \tag{B.5}$$

$$L = \bar{q}S\left(C_{L_0} + C_{L_\alpha}\alpha + C_{L_{\delta_e}}\delta_e\right), \tag{B.6}$$

$$\ell = \bar{q}Sb\left(C_{l_\beta}\beta + C_{l_p}\frac{Pb}{2v} + C_{l_r}\frac{Rb}{2v} + C_{l_{\delta_a}}\delta_a + C_{l_{\delta_r}}\delta_r\right), \tag{B.7}$$

$$M = \bar{q}S\bar{c}\left(C_{M_0} + C_{M_\alpha}\alpha + C_{M_q}\frac{q\bar{c}}{2v} + C_{M_{\delta_e}}\delta_e\right), \tag{B.8}$$

$$N = \bar{q}Sb\left(C_{N_\beta}\beta + C_{N_p}\frac{Pb}{2v} + C_{N_r}\frac{Rb}{2v} + C_{N_{\delta_a}}\delta_a + C_{N_{\delta_r}}\delta_r\right), \tag{B.9}$$

$$T_w^b = \begin{pmatrix} \cos\alpha\cos\beta & -\cos\alpha\sin\beta & \sin\alpha \\ \sin\beta & \cos\beta & 0 \\ \sin\alpha\cos\beta & -\sin\alpha\sin\beta & \cos\alpha \end{pmatrix}, \tag{B.10}$$

where $\bar{q}$, $\bar{c}$, v, α, and β represent the dynamic pressure, the mean aerodynamic chord, the vehicle velocity relative to the wind, the angle of attack, and the sideslip angle, respectively. Besides, C_{i_j}s denote different aerodynamic coefficients, which have been determined according to the aerial robot geometry using the finite-element analysis (in OpenVSP), and then, they are refined by several real flight experiments performed in different flight conditions. The final values of the aerodynamic coefficients are given in Table B.4. It should be noted that the aerodynamic coefficients of an aircraft are not constant in real applications. For example, four aerodynamic coefficients, i.e., C_L, C_M, C_Y, and C_N have been determined in different angles of attacks and sideslip angles (using the Vortex Lattice Method). The obtained curves for these coefficients are illustrated in Fig. B.9. As seen, they indicate nonlinear behaviors in different flight conditions. By substituting the constant value of the above-mentioned coefficients in the simulation model with the obtained nonlinear functions, the tracking error, assuming an ideal flight condition, is obtained as 0.492 m, while, as reported in Table 3, the tracking error (at ideal flight condition) is 0.465 m using constant aerodynamic coefficients. It should be noted that the presence of actuator faults and external disturbances in the flight simulation results in a tracking error of 0.66 m, which demonstrates much more impact of actuator faults and external disturbances on system dynamics compared to aerodynamic coefficients' variations. Accordingly, the nonlinear behavior of the aerodynamic coefficients is negligible compared to uncertain terms considered in flight simulations, and thus we can use the constant values given in Table B.4 in the simulation model as an acceptable aerodynamic model.

B.2. Engine and propeller

The propulsive force and moments can be formulated as:

$$T = \sum_{i=1}^{8} T_i, \quad M_T = \sum_{i=1}^{8} r_i \times T_i \hat{x}, \tag{B.11}$$

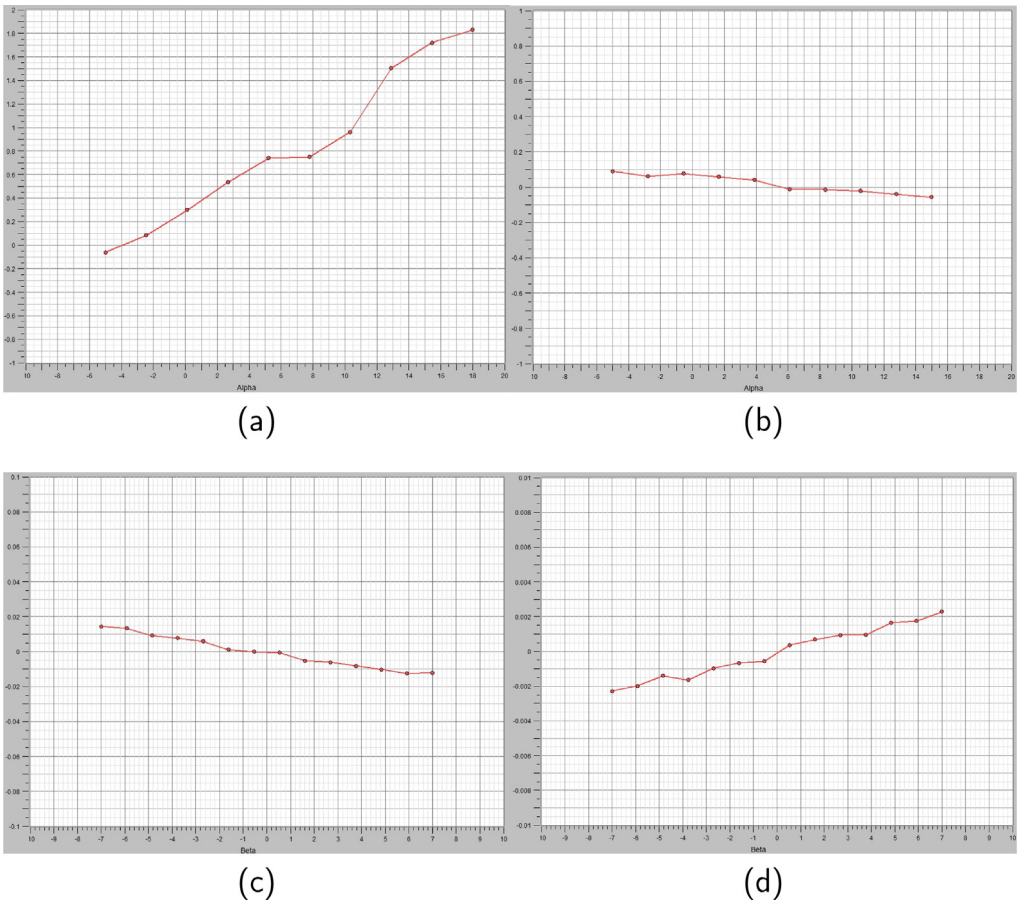

Fig. B.9. Computed aerodynamics coefficients using the finite-element analysis (which employs the Vortex Lattice Method), (a) C_L with respect to α, (b) C_M with respect to α, (c) C_Y with respect to β, (d) C_N with respect to β.

where T_i and r_i represent the thrust force and the location vector of each motor relative to the vehicle center of mass, respectively.

Remark 8. It is worth noting that the moments generated by asymmetric thrust forces of the motors on two sides of the aircraft (due to existing uncertainty in the dynamic model of each motor) are also considered in the model.

Further, the thrust force generated by each of the existing eight electric motors is in turn a nonlinear function of the throttle setting. To be more precise, the thrust force of each motor is computed as follows:

$$T_i = f_{th}(\delta_{th}, v, H) + N_{th}, \tag{B.12}$$

where f_{th} represents a nonlinear function of the throttle setting, the aircraft velocity, and the aircraft altitude. In this research, this function is computed numerically using the system identification method applied to real test data. E-max brushless electric motors equipped with 10×6 propellers have been employed in this aerial robot. The data obtained for each motor (on the ground) are illustrated in Fig. B.10. Also, N_{th} is used to model the uncertain dynamics, which is defined as a random constant bias added to a Gaussian noise (Bonfè, Castaldi, Geri, & Simani, 2006).

B.3. Actuator dynamics

Conventional actuators have been used in the current aircraft. Thus, it is possible to employ an appropriate classical dynamic model introduced for actuators in the literature (Collinson, 2011; Fadel, Rabie, & Youssef, 2019; Stevens et al., 2015). Second-order linear transfer functions with a natural frequency of 30 rad/s and a damping ratio of 0.7 have been employed to model the dynamics of the elevator, aileron, and rudder actuators. In addition, the upper/lower limit of the change rate of all actuators has been limited to ±90 deg/s, whereas the upper/lower limit of each actuator has been set to ±30 deg. Besides, the throttle actuator has been modeled as a linear first-order transfer function.

Table B.4
Computed values for the aerodynamic coefficients of the intended aerial robot.

Parameter	Value	Parameter	Value
C_{L_0}	0.34	C_{L_α}	0.096 (/deg)
C_{D_0}	0.0318	C_{D_α}	0.0075 (/deg)
C_{M_0}	0.05	C_{M_α}	−0.0143 (/deg)
$C_{L_{\delta_e}}$	0.305	$C_{D_{\delta_e}}$	0.0011
$C_{M_{\delta_e}}$	0.88	C_{L_q}	7.69
C_{M_q}	−30.57	C_{M_α}	−7.0
C_{l_β}	−0.023	$C_{l_{\delta_a}}$	0.139
$C_{l_{\delta_r}}$	0.0231	C_{l_p}	−0.598
C_{l_r}	0.111	C_{N_r}	−0.0311
C_{N_β}	0.028	$C_{N_{\delta_a}}$	−0.005
$C_{N_{\delta_r}}$	−0.04	C_{N_p}	−0.032
C_{Y_β}	−0.115	$C_{Y_{\delta_a}}$	0.005
$C_{Y_{\delta_r}}$	0.157	C_{Y_p}	−0.0414
C_{Y_r}	−0.126		

B.4. Reliability of the model

Finally, concerning the reliability of the model, it is worth mentioning that all the gravitational, propulsive, and aerodynamic forces and

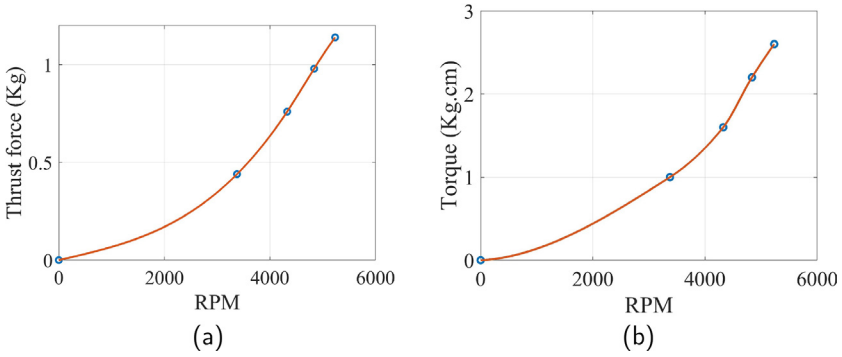

Fig. B.10. Obtained data for each motor, (a) generated thrust force with respect to RPM, (b) generated torque with respect to RPM.

moments have been modeled accurately using the data obtained from the finite-element analysis (in openVSP) integrated with the information extracted from several real flight experiments. Actuator dynamics and sensor noises have been carefully modeled, as well. In addition, as usual in the literature, the required system states in the proposed control approach include the velocity of the air vehicle in the inertial frame, the angular velocity, and the Euler angles, while they can be computed using the measurements from appropriate accelerometers and gyroscopes.

Besides, different uncertain terms including atmospheric disturbances, actuator faults, engine noise, measurement noises, and up to 20% random uncertainty in about all the aerodynamic coefficients and geometrical properties have been applied to the dynamic model of the aerial robot. This, in turn, results in a realistic dynamic model, which is representative of a genuine application.

References

Abbaspour, A., Aboutalebi, P., Yen, K. K., & Sargolzaei, A. (2017). Neural adaptive observer-based sensor and actuator fault detection in nonlinear systems: Application in UAV. *ISA Transactions*, *67*, 317–329. http://dx.doi.org/10.1016/j.isatra.2016.11.005.

Ali Emami, S., & Banazadeh, A. (2020). Fault–tolerant predictive trajectory tracking of an air vehicle based on acceleration control. *IET Control Theory & Applications*, *14*(5), 750–762. http://dx.doi.org/10.1049/iet-cta.2019.0596.

Arabi, E., Yucelen, T., Gruenwald, B. C., Fravolini, M., Balakrishnan, S., & Nguyen, N. T. (2019). A neuroadaptive architecture for model reference control of uncertain dynamical systems with performance guarantees. *Systems & Control Letters*, *125*(4), 37–44. http://dx.doi.org/10.1016/j.sysconle.2019.01.005.

Bonfè, M., Castaldi, P., Geri, W., & Simani, S. (2006). Fault detection and isolation for on-board sensors of a general aviation aircraft. *International Journal of Adaptive Control and Signal Processing*, *20*(8), 381–408. http://dx.doi.org/10.1002/acs.906.

Campa, G., Fravolini, M. L., Seanor, B., Napolitano, M. R., Gobbo, D. D., Yu, G., et al. (2002). On-line learning neural networks for sensor validation for the flight control system of a B777 research scale model. *International Journal of Robust and Nonlinear Control*, *12*(11), 987–1007. http://dx.doi.org/10.1002/rnc.728.

Chakrabortty, A., & Arcak, M. (2009). Robust stabilization and performance recovery of nonlinear systems with unmodeled dynamics. *IEEE Transactions on Automatic Control*, *54*(6), 1351–1356. http://dx.doi.org/10.1109/TAC.2009.2015554.

Chen, M., Shi, P., & Lim, C.-C. (2016). Adaptive neural fault-tolerant control of a 3-DOF model helicopter system. *IEEE Transactions on Systems, Man, and Cybernetics: Systems*, *46*(2), 260–270. http://dx.doi.org/10.1109/TSMC.2015.2426140.

Chowdhary, G., Johnson, E. N., Chandramohan, R., Kimbrell, M. S., & Calise, A. (2013). Guidance and control of airplanes under actuator failures and severe structural damage. *Journal of Guidance, Control, and Dynamics*, *36*(4), 1093–1104. http://dx.doi.org/10.2514/1.58028.

Chowdhary, G., Mühlegg, M., & Johnson, E. (2014). Exponential parameter and tracking error convergence guarantees for adaptive controllers without persistency of excitation. *International Journal of Control*, *87*(8), 1583–1603. http://dx.doi.org/10.1080/00207179.2014.880128.

Collinson, R. P. G. (2011). *Introduction to avionics systems* (3rd ed.). Dordrecht and London: Springer.

Ducard, G. J. J. (2009). *Advances in industrial control, Fault-tolerant flight control and guidance systems: practical methods for small unmanned aerial vehicles*. Dordrecht and London: Springer.

Emami, S. A., & Banazadeh, A. (2016). Control oriented modeling and identification of nonlinear systems. *Applied Mechanics and Materials*, *841*, 330–337. http://dx.doi.org/10.4028/www.scientific.net/AMM.841.330.

Emami, S. A., & Banazadeh, A. (2019). Intelligent trajectory tracking of an aircraft in the presence of internal and external disturbances. *International Journal of Robust and Nonlinear Control*, *29*(16), 5820–5844. http://dx.doi.org/10.1002/rnc.4698.

Emami, S. A., Castaldi, P., & Banazadeh, A. (2022). Neural network-based flight control systems: Present and future. *Annual Reviews in Control*, *53*(4), 97–137. http://dx.doi.org/10.1016/j.arcontrol.2022.04.006.

Emami, S. A., & Rezaeizadeh, A. (2018). Adaptive model predictive control-based attitude and trajectory tracking of a VTOL aircraft. *IET Control Theory & Applications*, *12*(15), 2031–2042. http://dx.doi.org/10.1049/iet-cta.2017.1048.

Emami, S. A., & Roudbari, A. (2019). Multimodel ELM-based identification of an aircraft dynamics in the entire flight envelope. *IEEE Transactions on Aerospace and Electronic Systems*, *55*(5), 2181–2194. http://dx.doi.org/10.1109/TAES.2018.2883848.

Fadel, M. Z., Rabie, M. G., & Youssef, A. M. (2019). Motion control of an aircraft electro-hydraulic servo actuator. *IOP Conference Series: Materials Science and Engineering*, *610*, Article 012073. http://dx.doi.org/10.1088/1757-899X/610/1/012073.

Fu, C., Hong, W., Lu, H., Zhang, L., Guo, X., & Tian, Y. (2018). Adaptive robust backstepping attitude control for a multi-rotor unmanned aerial vehicle with time-varying output constraints. *Aerospace Science and Technology*, *78*, 593–603. http://dx.doi.org/10.1016/j.ast.2018.05.021.

Galffy, A., Böck, M., & Kugi, A. (2019). Nonlinear 3D path following control of a fixed-wing aircraft based on acceleration control. *Control Engineering Practice*, *86*, 56–69. http://dx.doi.org/10.1016/j.conengprac.2019.03.006.

Ge, S. S., & Wang, C. (2002). Direct adaptive NN control of a class of nonlinear systems. *IEEE Transactions on Neural Networks*, *13*(1), 214–221. http://dx.doi.org/10.1109/72.977306.

Gomi, H., & Kawato, M. (1993). Neural network control for a closed-loop System using Feedback-error-learning. *Neural Networks*, *6*(7), 933–946. http://dx.doi.org/10.1016/S0893-6080(09)80004-X.

Gu, W., Valavanis, K. P., Rutherford, M. J., & Rizzo, A. (2019). A survey of artificial neural networks with model-based control techniques for flight control of unmanned aerial vehicles. In *2019 International conference on unmanned aircraft systems (ICUAS)* (pp. 362–371). Atlanta, GA, USA: IEEE, http://dx.doi.org/10.1109/ICUAS.2019.8797853.

He, W., Yan, Z., Sun, C., & Chen, Y. (2017). Adaptive neural network control of a flapping wing micro aerial vehicle with disturbance observer. *IEEE Transactions on Cybernetics*, *47*(10), 3452–3465. http://dx.doi.org/10.1109/TCYB.2017.2720801.

Huang, G.-B., Zhu, Q.-Y., & Siew, C.-K. (2006). Extreme learning machine: Theory and applications. *Neurocomputing*, *70*(1–3), 489–501. http://dx.doi.org/10.1016/j.neucom.2005.12.126.

Ioannou, P. A., Annaswamy, A. M., Narendra, K. S., Jafari, S., Rudd, L., Ortega, R., et al. (2014). L1-adaptive control: Stability, robustness, and interpretations. *IEEE Transactions on Automatic Control*, *59*(11), 3075–3080. http://dx.doi.org/10.1109/TAC.2014.2318871.

Ioannou, P. A., & Sun, J. (2012). *Robust adaptive control*. Mineola New York: Dover Publications Inc.

Kacprzyk, J., Schumann, J., & Liu, Y. (Eds.), (2010). *Studies in computational intelligence*, *Applications of neural networks in high assurance systems*. Berlin, Heidelberg: Springer Berlin Heidelberg, http://dx.doi.org/10.1007/978-3-642-10690-3.

Khalil, H. K. (2008). High-gain observers in nonlinear feedback control. In *International conference on control, automation and systems 2008*. Seoul, Korea.

Lai, G., Liu, Z., Zhang, Y., & Chen, C. L. P. (2016). Adaptive position/attitude tracking control of aerial robot with unknown inertial matrix based on a new robust neural identifier. *IEEE Transactions on Neural Networks and Learning Systems*, *27*(1), 18–31. http://dx.doi.org/10.1109/TNNLS.2015.2406812.

Lee, C. C. (1990). Fuzzy logic in control systems: Fuzzy logic controller. I. *IEEE Transactions on Systems, Man, and Cybernetics*, *20*(2), 404–418. http://dx.doi.org/10.1109/21.52551.

Li, Y., Hou, M., Liang, S., & Jiao, G. (2020). Predefined-time adaptive fault-tolerant control of hypersonic flight vehicles without overparameterization. *Aerospace Science and Technology*, *104*, Article 105987. http://dx.doi.org/10.1016/j.ast.2020.105987.

Liang, N.-Y., Huang, G.-B., Saratchandran, P., & Sundararajan, N. (2006). A fast and accurate online sequential learning algorithm for feedforward networks. *IEEE Transactions on Neural Networks*, *17*(6), 1411–1423. http://dx.doi.org/10.1109/TNN.2006.880583.

Lungu, M. (2020). Auto-landing of UAVs with variable centre of mass using the backstepping and dynamic inversion control. *Aerospace Science and Technology*, *103*(2), Article 105912. http://dx.doi.org/10.1016/j.ast.2020.105912.

MacKunis, W., Leve, F., Patre, P. M., Fitz-Coy, N., & Dixon, W. E. (2016). Adaptive neural network-based satellite attitude control in the presence of CMG uncertainty. *Aerospace Science and Technology*, *54*, 218–228. http://dx.doi.org/10.1016/j.ast.2016.04.022.

Narendra, K. S., & Annaswamy, A. M. (1987). A new adaptive law for robust adaptation without persistent excitation. *IEEE Transactions on Automatic Control*, 1067–1072. http://dx.doi.org/10.23919/ACC.1986.4789092.

Nguyen, N., Krishnakumar, K., Kaneshige, J., & Nespeca, P. (2008). Flight dynamics and hybrid adaptive control of damaged aircraft. *Journal of Guidance, Control, and Dynamics*, *31*(3), 751–764. http://dx.doi.org/10.2514/1.28142.

Patre, P. M., MacKunis, W., Kaiser, K., & Dixon, W. E. (2008). Asymptotic tracking for uncertain dynamic systems via a multilayer neural network feedforward and RISE feedback control structure. *IEEE Transactions on Automatic Control*, *53*(9), 2180–2185. http://dx.doi.org/10.1109/TAC.2008.930200.

Pi, C.-H., Hu, K.-C., Cheng, S., & Wu, I.-C. (2020). Low-level autonomous control and tracking of quadrotor using reinforcement learning. *Control Engineering Practice*, *95*(4), Article 104222. http://dx.doi.org/10.1016/j.conengprac.2019.104222.

Polycarpou, M. M. (1996). Stable adaptive neural control scheme for nonlinear systems. *IEEE Transactions on Automatic Control*, *41*(3), 447–451. http://dx.doi.org/10.1109/9.486648.

Pourtakdoust, S. H., Kiani, M., & Hassanpour, A. (2011). Optimal trajectory planning for flight through microburst wind shears. *Aerospace Science and Technology*, *15*(7), 567–576. http://dx.doi.org/10.1016/j.ast.2010.11.002.

Rysdyk, R., & Calise, A. J. (2005). Robust nonlinear adaptive flight control for consistent handling qualities. *IEEE Transactions on Control Systems Technology*, *13*(6), 896–910. http://dx.doi.org/10.1109/TCST.2005.854345.

Seshagiri, S., & Khalil, H. K. (2000). Output feedback control of nonlinear systems using RBF neural networks. *IEEE Transactions on Neural Networks*, *11*(1), 69–79. http://dx.doi.org/10.1109/72.822511.

Sonneveldt, L., van Oort, E. R., Chu, Q. P., & Mulder, J. A. (2009). Nonlinear adaptive trajectory control applied to an F-16 model. *Journal of Guidance, Control, and Dynamics*, *32*(1), 25–39. http://dx.doi.org/10.2514/1.38785.

Stevens, B. L., Lewis, F. L., & Johnson, E. N. (2015). *Aircraft control and simulation: dynamics, controls design, and autonomous systems* (3rd ed.). Chichester, West Sussex: Wiley Blackwell, Brian L. Stevens, Frank L. Lewis, Eric N. Johnson.

Wang, D., Zong, Q., Tian, B., Shao, S., Zhang, X., & Zhao, X. (2018). Neural network disturbance observer-based distributed finite-time formation tracking control for multiple unmanned helicopters. *ISA Transactions*, *73*, 208–226. http://dx.doi.org/10.1016/j.isatra.2017.12.011.

Xian, B., Diao, C., Zhao, B., & Zhang, Y. (2015). Nonlinear robust output feedback tracking control of a quadrotor UAV using quaternion representation. *Nonlinear Dynamics*, *79*(4), 2735–2752. http://dx.doi.org/10.1007/s11071-014-1843-x.

Xu, B., Gao, D., & Wang, S. (2011). Adaptive neural control based on HGO for hypersonic flight vehicles. *Science China Information Sciences*, *54*(3), 511–520. http://dx.doi.org/10.1007/s11432-011-4189-8.

Xu, B., Shi, Z., Sun, F., & He, W. (2019). Barrier Lyapunov function based learning control of hypersonic flight vehicle with AOA constraint and actuator faults. *IEEE Transactions on Cybernetics*, *49*(3), 1047–1057. http://dx.doi.org/10.1109/TCYB.2018.2794972.

Xu, B., Shi, Z., Yang, C., & Sun, F. (2014). Composite neural dynamic surface control of a class of uncertain nonlinear systems in strict-feedback form. *IEEE Transactions on Cybernetics*, *44*(12), 2626–2634. http://dx.doi.org/10.1109/TCYB.2014.2311824.

Xu, B., Wang, D., Zhang, Y., & Shi, Z. (2017). DOB-based neural control of flexible hypersonic flight vehicle considering wind effects. *IEEE Transactions on Industrial Electronics*, *64*(11), 8676–8685. http://dx.doi.org/10.1109/TIE.2017.2703678.

Yu, Z., Zhang, Y., Jiang, B., Su, C.-Y., Fu, J., Jin, Y., et al. (2020). Decentralized fractional-order backstepping fault-tolerant control of multi-UAVs against actuator faults and wind effects. *Aerospace Science and Technology*, *104*(6), Article 105939. http://dx.doi.org/10.1016/j.ast.2020.105939.

Yu, Z., Zhang, Y., Jiang, B., Yu, X., Fu, J., Jin, Y., et al. (2020). Distributed adaptive fault-tolerant close formation flight control of multiple trailing fixed-wing UAVs. *ISA Transactions*, *106*, 181–199. http://dx.doi.org/10.1016/j.isatra.2020.07.005.

Zahmatkesh, M., Emami, S. A., Banazadeh, A., & Castaldi, P. (2022). Robust attitude control of an agile aircraft using improved Q-learning. *Actuators*, *11*(12), 374. http://dx.doi.org/10.3390/act11120374.

Zou, Y., & Zheng, Z. (2015). A robust adaptive RBFNN augmenting backstepping control approach for a model-scaled helicopter. *IEEE Transactions on Control Systems Technology*, *23*(6), 2344–2352. http://dx.doi.org/10.1109/TCST.2015.2396851.

Zuo, Z., & Wang, C. (2014). Adaptive trajectory tracking control of output constrained multi-rotors systems. *IET Control Theory & Applications*, *8*(13), 1163–1174. http://dx.doi.org/10.1049/iet-cta.2013.0949.